Ultrafast dynamics in van der Waals heterostructures

Chenhao Jin[1], Eric Yue Ma[2,3], Ouri Karni[2], Emma C. Regan[1,4,5], Feng Wang[1,5,6*] and Tony F. Heinz[2,3*]

Van der Waals heterostructures are synthetic quantum materials composed of stacks of atomically thin two-dimensional (2D) layers. Because the electrons in the atomically thin 2D layers are exposed to layer-to-layer coupling, the properties of van der Waals heterostructures are defined not only by the constituent monolayers, but also by the interactions between the layers. Many fascinating electrical, optical and magnetic properties have recently been reported in different types of van der Waals heterostructures. In this Review, we focus on unique excited-state dynamics in transition metal dichalcogenide (TMDC) heterostructures. TMDC monolayers are the most widely studied 2D semiconductors, featuring prominent exciton states and accessibility to the valley degree of freedom. Many TMDC heterostructures are characterized by a staggered band alignment. This band alignment has profound effects on the evolution of the excited states in heterostructures, including ultrafast charge transfer between the layers, the formation of interlayer excitons, and the existence of long-lived spin and valley polarization in resident carriers. Here we review recent experimental and theoretical efforts to elucidate electron dynamics in TMDC heterostructures, extending from timescales of femtoseconds to microseconds, and comment on the relevance of these effects for potential applications in optoelectronic, valleytronic and spintronic devices.

Advances in the isolation and manipulation of atomically thin sheets of 2D crystals, starting with the investigations of graphene a decade ago, have ushered in a new era of basic scientific research and technological innovation. Two-dimensional layers with diverse properties can now be prepared separately and then stacked together to form new types of quantum materials, known as van der Waals (vdW) heterostructures. The ability to combine materials with monolayer precision enables the design and creation of functional 2D materials that do not exist in nature. Today, we have at our disposal a wide variety of atomically thin 2D layers, ranging from semiconducting MoS_2 and insulating hexagonal boron nitride (h-BN) to magnetic CrI_3 and superconducting $NbSe_2$, that can be stacked one upon the other. Because the electrons in atomically thin layers are exposed, different quantum states found in the individual layers can interact and couple to one another in ways that are not possible in other systems.

Such heterostructures constitute a vast family of new quantum materials, as they are defined not only by the combination of constituent monolayer materials, but also by the stacking sequence and relative crystallographic alignment of the layers. Further control of physical properties in 2D vdW heterostructures can be achieved through the application of electrostatic gating and fields, as well as substrate and strain engineering. Many fascinating physical phenomena have been reported in different vdW heterostructures, as exemplified by transport measurements revealing Hofstadter butterfly states, fractional Chern insulators, gate-tunable Mott insulators and unconventional superconductivity, amongst other effects[1–7]. In addition to electrical transport, there has also been great progress in the study of the optical properties and excited-state dynamics in vdW heterostructures. Here we review the new dynamical phenomena that emerge in semiconducting vdW heterostructures composed of stacked TMDC layers. We focus our discussion on TMDC heterostructures because the individual TMDC layers, with their many distinctive and intriguing properties, have already been well characterized and provide a strong basis for understanding the emergent new properties of heterostructures.

TMDC semiconductors (MX_2 layers with 2H symmetry and M = Mo, W; X = S, Se, Te) exhibit direct gaps at monolayer thickness. They feature strong interactions between light and matter, and greatly enhanced electron–electron interactions, with the optical properties largely defined by exciton states (bound electron–hole states). The exciton binding energies in monolayer TMDCs are hundreds of millielectronvolts—as much as two orders of magnitude larger than in typical bulk semiconductors such as silicon or GaAs (refs [8,9]). In addition, TMDC monolayers provide an excellent platform to investigate and control the valley degree of freedom associated with the energetically degenerate K and K′ valleys, which are formed as the extrema in the Brillouin zone of the valence and conduction bands. For TMDC monolayers, this binary valley degree of freedom—often designated as the valley pseudospin—is readily accessible optically as a consequence of the valley circular dichroism. The valley pseudospin in TMDC is, moreover, coupled to the electron/hole spin because of strong spin–orbit interactions[10,11].

Understanding the dynamic interplay and evolution of the charge, spin and valley excitations in vdW heterostructures is of fundamental scientific interest. It is also of central importance for many potential applications of TMDC materials in optoelectronics, spintronics and valleytronics. The dissociation of optically created excitons into free carriers is, for example, critical for photovoltaic devices, and the ability to control and stabilize valley polarization is essential for valleytronic applications. The formation of vdW heterostructures in TMDC layers can profoundly affect their excited-state dynamics, ranging from the dissociation of intralayer excitons and the formation of interlayer excitons to the relaxation of spin and valley polarization. The use of vdW heterostructures provides a powerful way to control and optimize the dynamic response of the constituent materials. In this Review, we survey recent progress in probing electron dynamics, extending from femtoseconds to microseconds, in TMDC heterostructures. On short timescales ($\lesssim$1ps), the dynamics is dominated by the charge transfer and energy relaxation processes in the heterostructure. On longer timescales ($\gtrsim$1ps),

[1]Department of Physics, University of California at Berkeley, Berkeley, CA, USA. [2]Department of Applied Physics, Stanford University, Stanford, CA, USA. [3]SLAC National Accelerator Laboratory, Menlo Park, CA, USA. [4]Graduate Group in Applied Science and Technology, University of California at Berkeley, Berkeley, CA, USA. [5]Material Science Division, Lawrence Berkeley National Laboratory, Berkeley, CA, USA. [6]Kavli Energy NanoSciences Institute at University of California Berkeley and Lawrence Berkeley National Laboratory, Berkeley, CA, USA. *e-mail: fengwang76@berkeley.edu; tony.heinz@stanford.edu

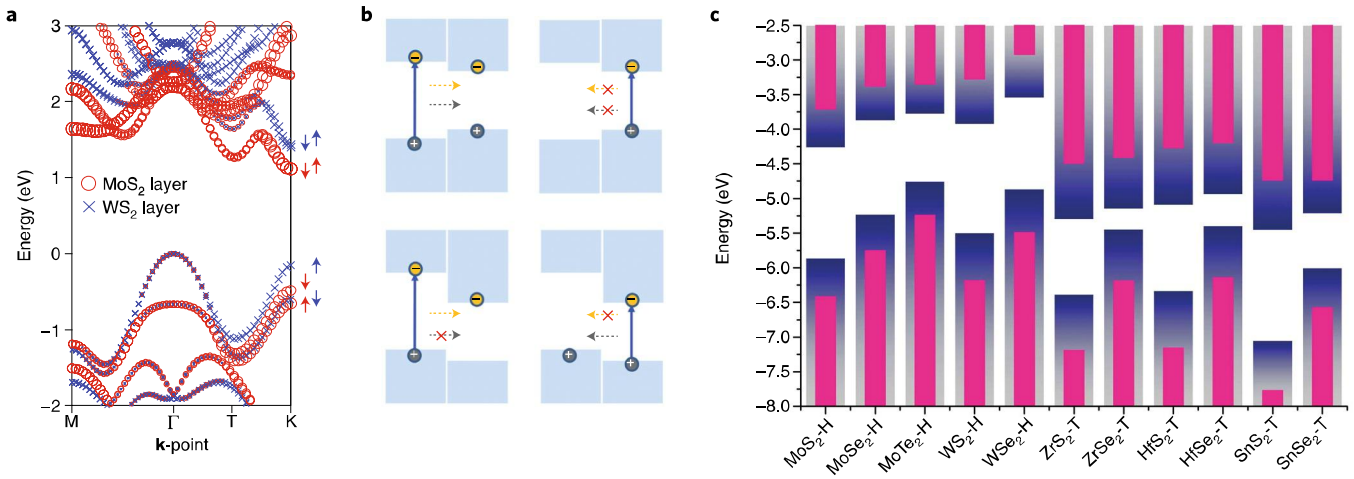

Fig. 1 | Band alignment in vertical vdW heterostructures of TMDCs. a, Calculated electronic states in a MoS_2/WS_2 vertical heterostructure, showing layer-localized states near the band edges at the K point[12]. **b**, Schematic of allowed charge transfer in heterostructures with type-I (top) and type-II (bottom) band alignment[16]. **c**, Calculated band-edge energies for various TMDCs[22] based on different theoretical treatments: ab initio density functional theory calculation using the Perdew–Burke–Ernzerhof functional (DFT-PBE) (blue) and G_0W_0 (pink). Adapted from ref. [12], APS (**a**); ref. [16], RSC (**b**); reproduced from ref. [22], IOP (**c**).

the recombination of interlayer excitons and relaxation of the spin and valley degrees of freedom become relevant. The rate of these processes can vary by orders of magnitude depending on the configuration, temperature and doping of the heterostructure. We will also touch on the dynamics of lateral transport of spin and valley polarization in TMDC heterostructures. We describe the physical mechanisms that underlie the different types of dynamic response in TMDC heterostructures and distinguish the behaviour from that of the constituent layers, as well as briefly mentioning the implications for potential new technologies.

Band alignment in TMDC heterostructures

In describing the single-particle electronic states in a vertical TMDC heterostructure, most authors consider the states to be largely localized within the individual layers. This approximation holds well for many electronic states close to the bandgap, owing to unusually weak interlayer coupling in TMDCs at the relevant K and K′ points in the Brillouin zone (Fig. 1a)[12]. Therefore, one can directly examine the relative energy difference, or band alignment, of material-specific electronic band extrema, just as is commonly done for heterostructures and quantum wells based on bulk materials[13,14]. An important distinction for atomically thin layers is that the concept of band bending near an interface does not apply[15].

Semiconductor heterostructures can have different types of band alignment depending on the energy difference of the conduction- and valence-band extrema in the constituent layers (Fig. 1b)[13,14]. The lowest-lying states for electrons and holes reside in the same layer for a type-I heterostructure[16], but are separated in different layers for a type-II heterostructure[13,17]. Further offsets in energy could, in principle, lower the conduction-band minimum (CBM) of one layer to a position below the valence-band maximum (VBM) of the other layer, yielding a type-III heterostructure[18].

The type of band alignment has profound effects on the excited-state dynamics in a vdW heterostructure. In a type-I heterostructure, carriers can only flow from the layer with the larger bandgap to the layer with the smaller bandgap (assuming that they do not have excess energy greater than the band offsets). The same applies to energy transfer through the exchange of virtual photons. In a type-II heterostructure, on the other hand, electrons accumulate in the layer with the lower CBM, while holes accumulate in the other layer[17,19,20]. Energy transfer can, however, still occur from the larger-gap to the smaller-gap material[21].

There have been numerous theoretical studies of the band alignment in TMDC heterostructures[13,14,18,22–24]. The result of one recent calculation is shown in Fig. 1c. Many of the theoretical studies make use of density functional theory (DFT) or related methods and cannot fully account for the effects of doping (Fermi-level difference), dielectric screening and excitonic interactions[25]. Nonetheless, they provide guidelines for realizing specific types of heterostructures and combination of bandgaps. Although theoretical studies are advancing rapidly, at present a definitive determination of heterostructure band alignment must rely on experiment[26,27].

In the following, we describe experimental findings concerning the dynamics of charge and energy transfer for representative TMDC heterostructures, followed by a summary of the relevant theoretical studies.

Experimental studies of charge and energy transfer

Following the predictions of type-II band alignment in TMDC heterostructures, several experimental studies aimed (among other goals) to validate these theoretical results by probing the associated charge transfer or energy transfer processes. Vertical heterostructures have been examined for various material combinations prepared by different fabrication methods, including stacking of layers exfoliated from bulk crystals and from layers grown by chemical vapour deposition (CVD), as well as direct heterostructure growth by CVD.

Ultrafast optical measurements using pump–probe spectroscopy provide the possibility of accessing charge and energy transfer processes with femtosecond time resolution. In initial experiments, Hong et al. examined the dynamics of the MoS_2/WS_2 heterostructure. Following excitation by an ultrafast laser pulse resonant with the lower-energy MoS_2 A exciton, they observed a transient change in reflectivity near the higher-energy WS_2 exciton (Fig. 2a)[19]. Based on theoretical predictions of type-II band alignment of the two materials, this transient response was attributed to charge transfer of a hole from the MoS_2 monolayer to the WS_2 monolayer. By deconvolving the instrument response from the rise-time of the signal, the authors were able to provide an upper limit of 50 fs for the charge transfer time. Ceballos et al. observed similar dynamics in a heterostructure of $MoS_2/MoSe_2$, without

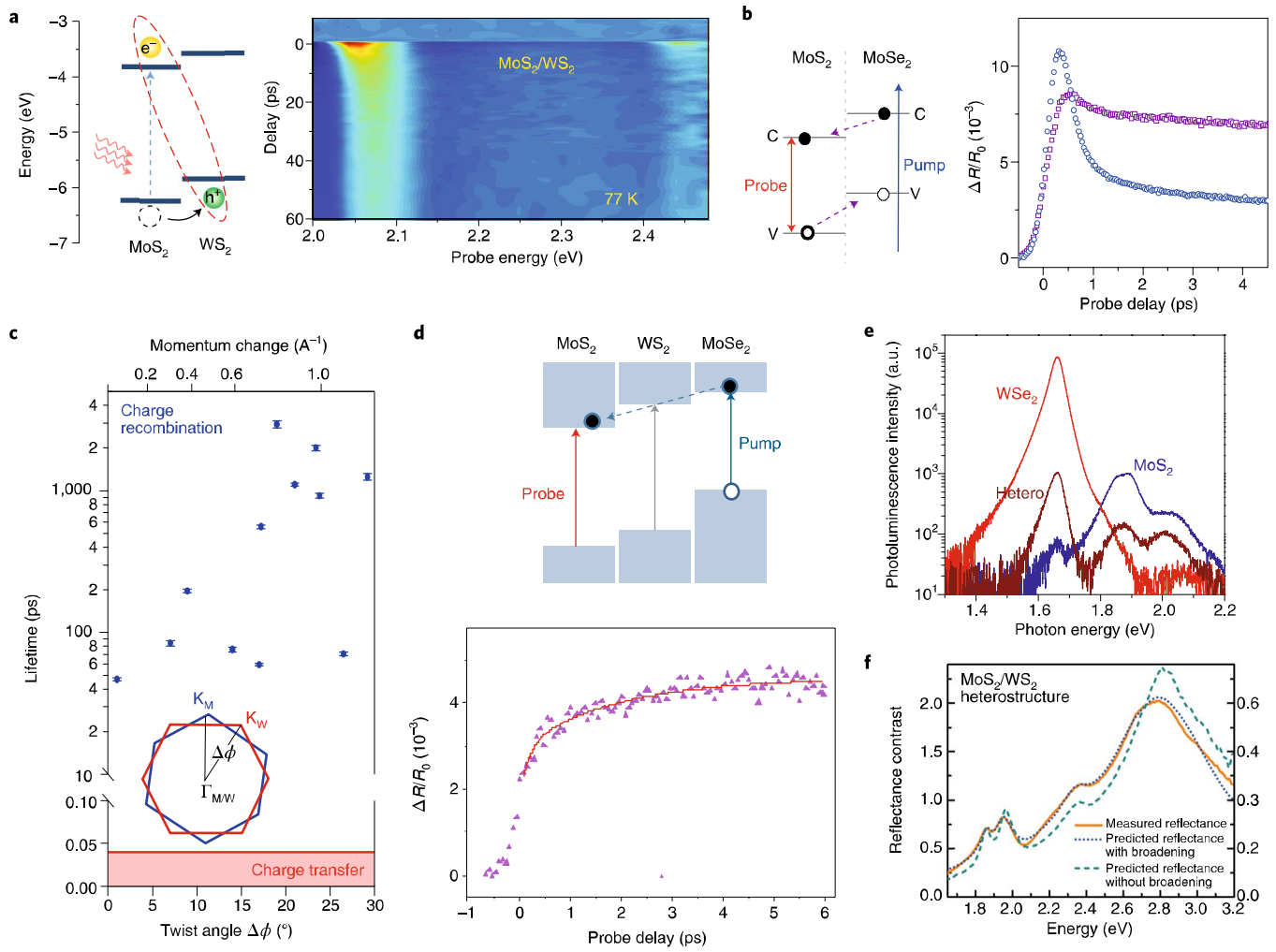

Fig. 2 | Experimental studies of ultrafast charge transfer in vertical TMDC heterostructures. a, Schematic and energy-resolved transient absorption spectra of a MoS_2/WS_2 heterostructure, excited by an optical pulse near the lower-energy MoS_2 A exciton feature, indicating hole transfer[19]. **b**, Schematic and time-resolved differential reflection of a $MoS_2/MoSe_2$ heterostructure (blue) and of monolayer MoS_2 (purple), excited by an optical pulse above the bandgaps of both materials, indicating both electron and hole transfer[28]. **c**, Charge transfer (red shading) and recombination (blue) times in heterostructures of MoS_2 and WSe_2 with different twist angles, as indicated[30]. Subscript W indicates WSe_2, M indicates MoS_2. **d**, Differential reflection at the energy of the MoS_2 A exciton following excitation at the energy of the $MoSe_2$ A exciton in a $MoSe_2/WS_2/MoS_2$ trilayer heterostructure[33]. **e**, Photoluminescence quenching[40] in MoS_2/WSe_2. The results are compared with the response of the separated monolayers. a.u., arbitrary units. **f**, Broadening of the absorption features[39] in a MoS_2/WS_2 heterostructure. Adapted from ref. [19], SNL (**a**); ref. [28], American Chemical Society (**b**); ref. [33], American Chemical Society (**d**); ref. [40], SNL (**e**); ref. [39], American Chemical Society (**f**). Reproduced from ref. [30], American Chemical Society (**c**).

spectrally resolving the reflection of the probe[28]. They concluded, based on the theoretically predicted band alignment, that electrons were transferred from $MoSe_2$ to MoS_2. In addition, when exciting both layers (using excitation resonant with the higher-energy exciton feature in MoS_2) and comparing the transient reflectivity signal of the monolayers to that of the heterostructure, the authors identified the presence of hole transfer in the opposite direction: that is, from MoS_2 to $MoSe_2$ (Fig. 2b).

Following these first experimental investigations, several groups examined the nature of the ultrafast charge transfer for different types of heterostructures under different conditions. Heo et al. compared CVD-grown and manually stacked WS_2/MoS_2 heterostructures with a focus on the dependence on the relative (twist) angle of the two constituent lattices[29]. Measuring the transient transmission of the probe signal, they did not resolve differences in the rise-time of the signal associated with charge transfer, but did observe a pronounced difference in the decay times of the signal. Wang et al. examined several WSe_2/WS_2 heterostructures composed of CVD-grown layers mechanically stacked with different twist angles[20]. Using pump–probe measurements, together with steady-state techniques such as reflection contrast spectroscopy, they showed the same ultrafast signature from the onset of charge transfer, either from electrons moving from WSe_2 to WS_2 or from holes travelling in the opposite direction. They concluded that interlayer charge transfer takes place within 450 fs, close to the duration of the pump pulses in their experiment, and does not exhibit measurable sensitivity to the twist angle. Further reinforcing this conclusion, Zhu et al. explored deterministically aligned heterostructures of mechanically exfoliated MoS_2 and WSe_2; they found that the charge transfer signal appeared within 40 fs regardless of twist angle (Fig. 2c)[30]. On the other hand, the timescale of the decay varied with the twist angle, but without any clear trend. Ji et al. reported a similar charge transfer rise-time for stacks of CVD-grown MoS_2 and WS_2 (ref. [31]). Such rapid interlayer charge transfer irrespective of crystal orientation (and thus crystal momentum) is somewhat unintuitive. Chen et al. probed intraband transitions in a heterostructure using

infrared light and suggested a potential explanation based on the rapid formation of 'hot' interlayer excitons[32]. Additional theoretical investigations are summarized in the next section.

Further demonstrating its robustness, the signature of picosecond electron transfer was observed in a trilayer heterostructure in which monolayers of $MoSe_2$ and MoS_2 were separated by a monolayer of WS_2 (Fig. 2d, ref. [33]). The authors suggested that such rapid charge transfer across multiple materials is coherent, rather than sequential.

Charge transfer dynamics was also revealed in investigations of the coupling between pairs of TMDC layers. Charge transfer in a $MoS_2/MoTe_2$ heterostructure was identified using pump–probe experiments[34], leading to the suggestion of $MoTe_2$ as a good electrical contact for other semiconducting TMDCs and metals. Later, cascaded transfer of electrons and holes across several TMDC heterostructures was invoked to explain correlated blinking observed in the photoluminescence in those stacks[35].

In addition to these time-resolved pump–probe measurements, charge transfer between two TMDC layers in a heterostructure has been inferred from quenching of the photoluminescence of the constituent monolayers[19,20,28–33,36–38] and by broadening of the resonant features in the monolayers in optical absorption measurements[20,39], both phenomena arising as a consequence of the presence of additional relaxation channels in the heterostructures. A reduction in the photoluminescence intensity by factor of a few tens to a few hundreds has commonly been observed (Fig. 2e)[19,40]. This suggests a corresponding ratio for the charge transfer time compared with the population lifetime in the isolated material. Assuming the latter to be a few hundred picoseconds for excitons in monolayer TMDCs[41] at room temperature, we estimate a charge transfer time of about 1 ps, somewhat longer than measured by pump–probe techniques. This discrepancy can be explained as the result of a small fraction of the heterostructure exhibiting poor contact between the layers, thus yielding reduced photoluminescence quenching compared with that of the ideal structure. In optical absorption measurements, linewidth broadening of heterostructures compared with that of the separate monolayers has been reported and used to estimate non-radiative decay rates comparable to those deduced from pump–probe experiments (Fig. 2f)[39]. Extrinsic factors, such as strain introduced in fabricating the heterostructure, can potentially also play a role. The extremely rapid (few femtosecond) relaxation times inferred for high-lying states may, however, remain difficult to probe directly in the time domain, but are easily observable by lineshape analysis.

Another dynamic process that may compete with charge transfer is energy transfer. In this latter process, an exciton created in one layer recombines, and the released energy creates an exciton in the other layer. Kozawa et al. reported evidence for such a process in a $MoSe_2/WS_2$ heterostructure (ref. [21]) on the basis of a measured enhancement of photoluminescence from the $MoSe_2$ feature under excitation resonant with the WS_2 optical bandgap. Recently, energy transfer was also identified in heterostructures of MoS_2 and WS_2 separated by insulating layers of h-BN[42]. In these structures, photoluminescence quenching from the heterostructure was reduced, or even became photoluminescence enhancement, upon increasing the thickness of the h-BN spacer. This was interpreted as an energy transfer process between B excitons in MoS_2 and A excitons in WS_2. The dependence of the enhancement on spacer thickness, with an optimum of photoluminescence enhancement for about five layers of h-BN and subsequent reduction of this effect with increasing layer thickness, is compatible with the predicted trend for a dipole–dipole interaction. This highlights the major difference between energy transfer and charge transfer processes: whereas the latter requires intimate coupling of the two constituent monolayers, the former, originating in dipole–dipole interactions, can act at greater distances and across insulating spacers. Although this difference between the processes is clear, there is currently little direct experimental information on the absolute rates of energy transfer for TMDC layers and in what regimes and under what conditions energy transfer competes with charge transfer.

Theoretical studies of charge and energy transfer

Because most experiments have excited and probed excitonic resonances of the constituent layers, it has often been assumed that charge transfer occurs between their direct band-edge (K/K′ valley) states. Band structure calculations have shown that the K/K′ states are localized around the central layer of metal atoms and have weak interlayer interactions. On the other hand, for states of different momentum, such as in the Γ or Q valleys, the interlayer coupling may be much stronger. One consequence of this difference is the transition from indirect to direct bandgap upon thinning TMDCs to the monolayer limit: the bulk CBM in the Q valley, more affected by interlayer coupling, lies above the K valley in monolayers[43,44]. For the same reason, the K-valley states are not expected to show such rapid interlayer charge transfer. This contradiction with experiment is further heightened by the apparent independence of charge transfer on twist angle and lattice mismatch, the factors that dictate the momentum difference between the initial and final states, as well as its insensitivity to temperature. Here we briefly survey some of the approaches presented in the literature to identify the mechanism responsible for the very efficient charge transfer processes observed experimentally in vertical TMDC heterostructures.

Zhu et al., following considerations relevant for charge transfer processes in molecular systems, have pointed out the possible role of localization in bridging the momentum mismatch[45]. The electrostatic attraction between the optically excited electron and hole, which leads to the formation of tightly bound excitons, gives rise to a distribution of momenta for the charge carriers across a considerable range of wavevectors in the Brillouin zone. This situation could explain the apparent lack of momentum conservation in the observed charge transfer process. However, it is unclear whether this effect alone could supply the large momentum required for charge transfer in heterostructures with large twist angles[30]. In addition, for excitation substantially above the bandgap, it is unclear whether exciton formation occurs before charge transfer[28].

Several groups have also used numerical calculations using molecular dynamics and time-dependent density-functional theory (TD-DFT) to elucidate the mechanism for interlayer charge transfer. Because accurately accounting for the effect of excitons is computationally demanding, these calculations have focused on the transfer of free charge carriers from one monolayer to its neighbour. Wang et al. described a process of transferring holes directly between the K valleys of the two layers mediated by the electric dipole interaction of the initial and final states, which enhances the coupling between the states to above a critical level for collective charge transfer[46]. In this description, both twist angle and temperature have a significant influence on the transfer rate[46]. Zhang et al. pointed out the significance of such dipole coupling between specific states in the vicinity of the K valley and highlighted the expected twist-angle dependence of the charge transfer rate[47]. Additionally, the authors argue that the omission of excitonic effects for above gap excitation may not be significant if the timescales for charge transfer and exciton formation are comparable. (This argument is, however, problematic for explaining charge transfer from excitons created directly by resonant excitation.)

A slightly different picture is presented by Long et al.[48] and by Li et al.[49] for charge transfer processes in $MoSe_2/MoS_2$ and MoS_2/WS_2 systems, respectively. They propose that holes and/or electrons undergo transfer from one layer to the other due to mixing between the electronic states near the K points of both layers[48,49]: the states into which the charge carriers are optically injected are coherently mixed (and therefore delocalized) across the two layers, so that charge transfer need only to be driven by an intralayer

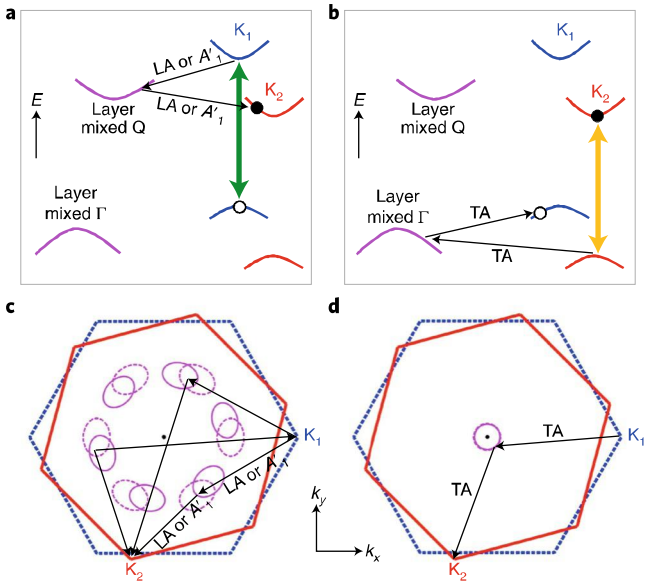

Fig. 3 | Theoretical concepts explaining the robust and ultrafast nature of charge transfer in TMDC heterostructures[52]. **a**, Schematic representation of phonon-mediated electron transfer. LA, longitudinal acoustic phonons; A'_1, a specific optical phonon. **b**, The same for hole transfer. TA, transverse optical phonons. **c**, Top view of the twisted Brillouin zones of the two layers, where electron transfer between the K points is mediated by phonon coupling to the Q point. **d**, The same for hole transfer, mediated in this case by the coupling to the Γ point. Adapted from ref. [52], APS.

relaxation process to the K valley, mediated by phonon emission. In this model, the coupling relies on specific layer orientations to assist the state mixing in the heterostructure. The discrepancy between this requirement and the apparent twist-angle independence of charge transfer in experiments is explained in terms of changes in the relative local atomic positions in the two layers across the moiré pattern of the heterostructure[50,51]. Regardless of the twist angle of the layers, such lateral inhomogeneity provides regions where the coupling between the layers is strong[31]. In all of the above scenarios, phonons are necessary for the completion of the charge transfer process, but not for its initiation.

Recent work has also explored a more direct role for phonons in the initiation of charge transfer. Wang et al. considered momentum-conserving charge transfer between the layers in various regions of the Brillouin zone, including at the K, Q and Γ points for different twist angles and degrees of lattice mismatch[52], as shown in Fig. 3a–d. The proposed mechanism involves scattering by phonons from the K valley to the Γ valley (for holes) or to the Q valley (for electrons), regions where the interlayer coupling is strong and interlayer charge transfer is rapid. After charge transfer, scattering with another phonon would bring the charge carriers back to the K valley. For intralayer scattering within 20 fs, the entire charge transfer process would occur in less than 100 fs, as observed experimentally. A similar scheme was developed by Zheng et al. using a numerical molecular dynamics TD-DFT calculation, although without accounting for the influence of the moiré pattern[53]. These theories better match the observed twist-angle independence, as the coupling around the Γ and Q points is not sensitive to the layer orientation. The expected temperature dependence of this mechanism is also weak, as it only requires emission of phonons to dissipate the excess energy available from the transfer. This general mechanism has been adopted in the interpretation of recent experiments related to charge transfer processes[30,33,37].

Spin and valley dynamics in TMDC heterostructures

The previous sections addressed carrier dynamics in TMDC heterostructures on the ultrafast timescale ($\lesssim$1ps) relevant for interlayer charge transfer in systems with type-II band alignment. In this section, we focus on spin and valley relaxation dynamics in TMDC heterostructures, which take place on considerably longer timescales.

Within a TMDC monolayer, there are two distinct relaxation processes to consider. First, the population decay of optically excited excitons has a characteristic timescale of few picoseconds to nanoseconds, depending on choice of material, sample preparation, temperature and so on[54–58]. Second, the exciton spin–valley lifetime, which determines how long information can be stored in the spin–valley degree of freedom, has been found to be a few picoseconds in isolated monolayer TMDCs[59–63]. Both the population and the spin–valley lifetimes in type-II heterostructures, where the electrons and holes reside in different layers after the rapid initial charge transfer process, can differ markedly from the corresponding lifetimes in isolated monolayers.

Below, we review recent experimental results on dynamics on the pico-to-microsecond timescale in heterostructures and show that both the population lifetime and the spin–valley lifetime can be significantly longer than for the monolayer case. We then summarize recent efforts towards understanding the physical mechanisms of the corresponding intervalley scattering processes. Finally, we discuss the spatio-temporal dynamics of spin and valley polarization in TMDC heterostructures.

Long spin and valley lifetime

Traditional electronic devices are based on the manipulation of electron charges in real space. Using other electron degrees of freedom as the information carrier, such as spin and valley, can potentially overcome fundamental limits of speed and power consumption, giving rise to intriguing new concepts in spintronics and valleytronics. A long spin or valley lifetime is necessary to ensure that the spin or valley information will be maintained in the idle state and can persist long enough to be processed. We note that the valley lifetime discussed here should not be confused with the valley depolarization time: the former can originate from different mechanisms, including the population decay of the valley information carriers, whereas the latter describes only the intervalley scattering process.

TMDCs offer a promising platform for spintronic and valleytronic applications, owing to several attractive properties of these materials. The valley-dependent optical selection rules allow for the convenient creation, manipulation and detection of excitons in specific valleys with circularly polarized light[64–66]. Furthermore, the spin–valley locking effect suggests that a very long spin–valley lifetime is possible because intervalley scattering of electrons or holes requires both a large momentum change from K to K′ and a simultaneous spin flip[10,11]. However, several groups have measured exciton spin–valley dynamics using time-resolved Kerr rotation (TRKR)[59–63], and the spin–valley lifetime in TMDC monolayers was found to be rather short, ranging from one to a few picoseconds, even at low temperatures. This counter-intuitive observation was later explained as a consequence of the exchange interaction between excitons in the two valleys[67–70]: a bright exciton always has total momentum and spin of zero and therefore does not require any change in momentum or spin to scatter to the other valley as an intact exciton. This reduced spin–valley lifetime of excitons in TMDC monolayers limits their use in carrying spin–valley information.

A general strategy for improving the spin–valley lifetime in TMDCs is to eliminate the exciton exchange interaction by converting excitons into other excitations that serve as alternative carriers of valley information. An additional figure of merit, the conversion efficiency, must then be introduced to quantify the final valley imbalance created from each optically excited exciton. To avoid

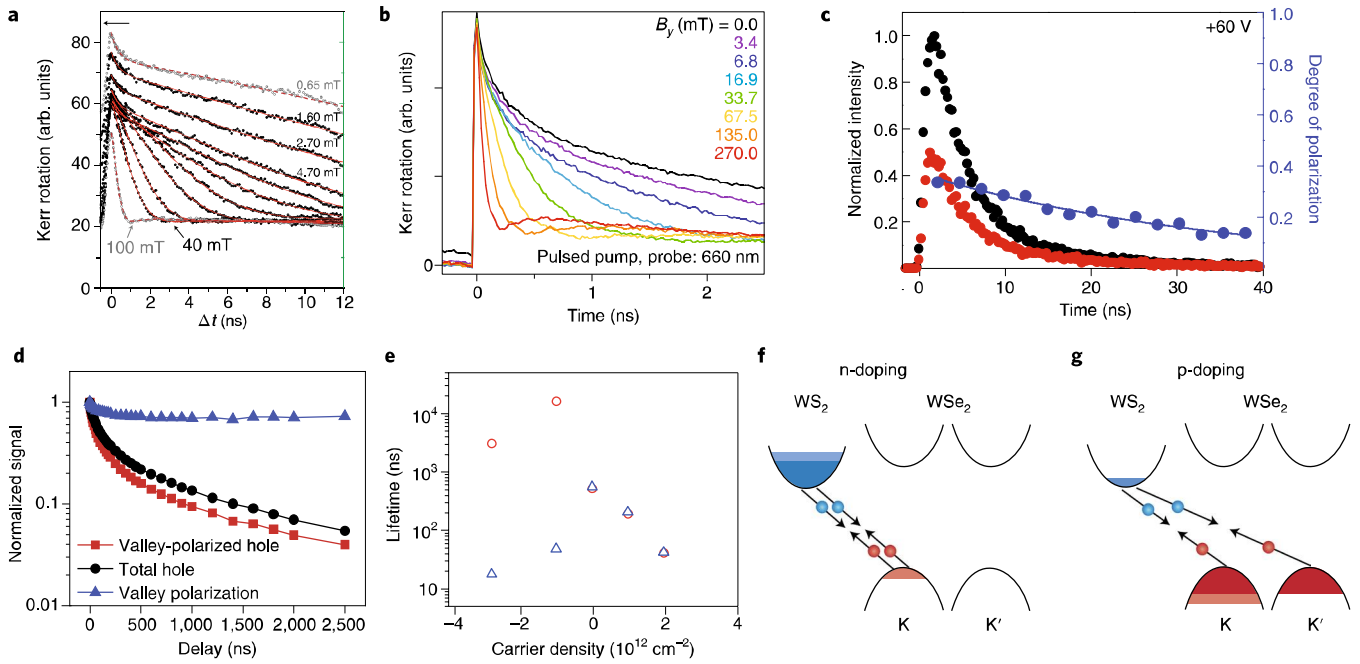

Fig. 4 | Dynamics of spin–valley information carriers in TMDC materials. a,**b**, Spin–valley dynamics of trions (**a**)[72] and resident electrons (**b**)[81] in monolayer TMDC materials under different external magnetic fields, as probed by time-resolved Kerr rotation measurements. A spin–valley lifetime of a few nanoseconds to tens of nanoseconds is observed at low fields. **c**, Time-resolved photoluminescence in a nearly aligned $WSe_2/MoSe_2$ heterobilayer for the same (black) and opposite (red) circularly polarized excitation as well as their ratio (blue), revealing a valley lifetime of few nanoseconds[84]. **d**, Decay dynamics of the valley-polarized hole population, the total hole population and the valley polarization in a large-twist-angle WSe_2/MoS_2 heterostructure at charge neutrality[94]. **e**, Summary of the hole population (blue) and spin–valley (red) lifetimes as a function of carrier concentration in a large-twist-angle WSe_2/WS_2 heterostructure[95]. **f**,**g**, Schematic illustration of the interlayer electron–hole recombination process in electron-doped (**f**) and hole-doped (**g**) heterostructures[95]. Adapted from ref. [72], APS (**a**); ref. [84], AAAS (**c**). Reproduced from ref. [81], SNL (**b**); ref. [94], AAAS (**d**); ref. [95], AAAS (**e**–**g**).

loss of valley information during conversion, the timescale of the conversion process (that is, the exciton population lifetime) must be comparable to or shorter than the picosecond spin–valley lifetime of excitons. In monolayer TMDCs, several candidates have been considered as the alternative information carriers, including trions[71–73], dark excitons[74,75], biexcitons[76,77] and resident carriers[78–81]. For example, Fig. 4a,b shows the valley dynamics of trions and resident electrons probed by TRKR measurement. Unlike bright excitons, these excitations have non-zero total momentum and/or total spin, and therefore will not suffer from rapid spin–valley relaxation through the exchange interaction. Their spin–valley lifetimes at low temperatures range from tens of picoseconds to a microsecond, but the conversion efficiency from the initially generated exciton has rarely been characterized. However, since the exciton population lifetime is comparable to or longer than the exciton spin–valley lifetime in these cases, the valley conversion efficiency is likely to be considerably less than unity.

On the other hand, the interlayer charge transfer process in type-II heterostructures provides an attractive mechanism to transform intralayer excitons on the femtosecond timescale. As discussed above, the ultrafast charge transfer process occurs very rapidly, typically within 50 fs, in TMDC heterostructures[19,82]. Because this timescale is much faster than exciton spin–valley relaxation, the loss of spin–valley information during the conversion process is expected to be minor.

In nearly aligned heterobilayers, electrons and holes can form bright interlayer excitons after the charge transfer process[28,38,83]. Rivera et al. observed 40% positive circular polarization from interlayer exciton emission in a $WSe_2/MoSe_2$ bilayer and measured a spin–valley lifetime of a few nanoseconds in a time-resolved photoluminescence study[84], as shown in Fig. 4c. The significantly longer spin–valley lifetime of interlayer excitons can be understood by noting that the electron and hole wavefunctions have much smaller overlap in interlayer excitons than in intralayer excitons; they will therefore have a weaker exchange interaction and exhibit slower recombination processes (both radiative and non-radiative).

Recently, there has been increasing research interest in the nature of the interlayer exciton state and the origin of the circular polarization of its emission in nearly aligned heterostructures. Hsu et al. reported negative helicity of interlayer exciton emission[85] in a $WSe_2/MoSe_2$ bilayer, while Hanbicki et al. and Ciarrocchi et al. observed two separate interlayer exciton emission peaks with opposite signs of helicity[86,87]. Meanwhile, various configurations of interlayer excitons have been proposed as the emitting state, including spin-singlet zero-momentum excitons[84,88], spin-triplet zero-momentum excitons[89] and finite-momentum excitons[90,91]. The rich set of observations originates in part from the complex conduction band structure in the $WSe_2/MoSe_2$ heterostructure, where electron states of spin up and spin down, and at K and Q valleys, are all close in energy. Furthermore, the real-space distribution of interlayer excitons when a moiré pattern is present can further modify the optical selection rules[92,93]. The exact mechanisms behind these interesting observations are yet to be fully understood.

An alternative approach involves using single-particle states, such as holes in WSe_2, to carry valley information in the heterostructure. Because the momentum match between electrons and holes (required for efficient exciton emission) is not relevant in this approach, a large-twist-angle bilayer is preferred to separate electrons and holes in momentum space and further reduce their exchange interaction and recombination rate. Kim et al. measured the spin–valley lifetime of holes in WSe_2/MoS_2 heterostructures

using circularly polarized pump-probe spectroscopy[94]. Figure 4d shows the measured decay dynamics of the total hole population and valley-polarized hole population in the WSe_2 layer at a temperature of 10 K. Both the population and the spin–valley lifetimes of holes are around a microsecond, indicating that the decay of the spin–valley imbalance occurs primarily through population loss. On the other hand, the valley polarization remains almost constant for a few microseconds, from which one can extract a valley depolarization time (or intervalley scattering time) exceeding 40 μs. The other critical figure of merit, the conversion efficiency, was also determined experimentally to be close to unity for valley-polarized holes[94]. The nearly ideal conversion efficiency is consistent with an interlayer charge transfer process that is far faster than intervalley scattering processes.

The spin–valley lifetime of resident holes in the heterostructure can be further improved by tuning the carrier concentration. Figure 4e summarizes the doping-dependent spin–valley lifetime of holes in a WSe_2/WS_2 heterostructure (red circles), as compared to the population lifetime of holes (blue triangles)[95]. In charge-neutral and electron-doped heterostructures, the spin–valley lifetime is similar to the population lifetime; however, for hole-doping, the spin–valley lifetime becomes orders of magnitude longer than the population lifetime. This doping dependence is a consequence of the interlayer electron–hole recombination process, as shown in Fig. 4f,g. For electron-doped or charge neutral heterostructures (Fig. 4f), all the holes in WSe_2 are pump-generated excess holes. Therefore, when the hole population decays to zero owing to interlayer electron–hole recombination, no holes—and certainly no valley-polarized holes—remain in the WSe_2. The valley lifetime is then limited by the lifetime of the total hole excess. On the other hand, if the original hole density is much greater than the photogenerated density, excess electrons in WS_2 will recombine with holes from both valleys of WSe_2 with nearly equal probability (Fig. 4g). Consequently, a pure spin–valley imbalance (that is, equal excess and deficiency of holes in the K and K′ valleys) is generated, the lifetime of which can be much longer than the population lifetime and has been found to exceed 20 μs. Furthermore, the decrease of spin–valley imbalance is negligible during the population decay, and the overall efficiency of this two-step conversion process can approach 100%[95].

Potential mechanism for intervalley scattering

As discussed in the previous sections, the spin–valley lifetime can be limited either by the population lifetime or by the intervalley scattering process. The first limitation can be removed for valley-polarized holes in hole-doped heterostructures, making them promising candidates for spin–valley information carriers. Furthermore, directly probing hole dynamics provides relatively clean information about the decay mechanism owing to the simplicity of the valence band maximum. This configuration thus provides a valuable platform for understanding intervalley scattering processes in TMDC materials.

Figure 5a shows the decay dynamics of valley polarization at different temperatures for holes in WSe_2/MoS_2 heterostructures, with the valley depolarization lifetime summarized in Fig. 5b (ref. [94]). The depolarization lifetime increases from 10 ns at 77 K to above 40 μs at 10 K, which roughly follows a thermally activated rate: $\tau \propto \exp\left(\frac{\Delta}{k_B T}\right)$, with k_B denoting the Boltzmann constant and $\Delta \approx 20$ meV.

The intervalley scattering of holes in WSe_2 requires a large momentum change and a simultaneous spin flip. However, owing to the strong spin–orbit coupling in WSe_2, the picture of electrons and holes with perfectly defined up and down spin states in the K and K′ valleys, respectively, is not strictly valid for states away from the K and K′ points. Therefore, intervalley scattering of carriers near but not exactly at K and K′ points is allowed. This process, often designated as the Elliott–Yafet mechanism, has a characteristic temperature dependence

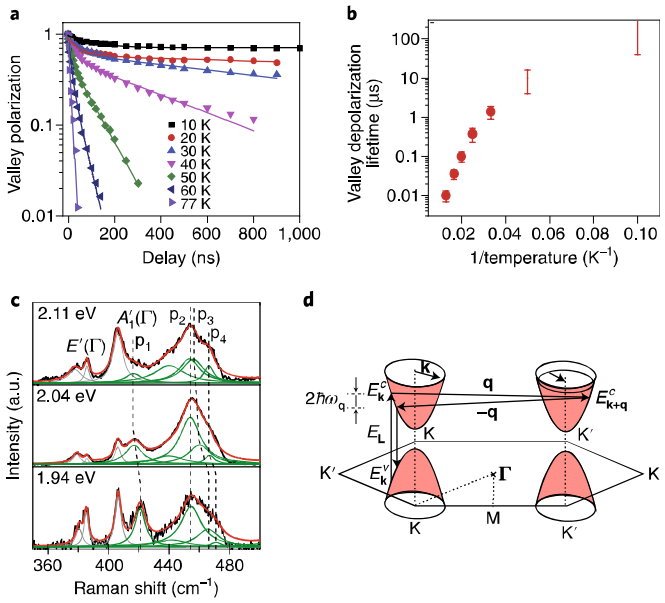

Fig. 5 | Potential origin of intervalley scattering in WSe_2/MoS_2 heterostructures. a, Temperature-dependent decay dynamics of valley polarization. **b**, Temperature dependence of the intervalley scattering time. The process can be described as thermally activated[94]. **c**,**d**, Resonant Raman spectra (**c**) of single-layer MoS_2 show particularly strong second-order Raman signals (peaks p1 to p4) for excitation around 2.0 eV through a doubly resonant Raman process involving K-point phonons, as illustrated in **d**[96]. E_L, energy of excitation light. Reproduced from ref. [94], AAAS (**a**,**b**); ref. [96], SNL (**c**,**d**).

of $\tau_{EY}^{-1} \propto T^2\ \tau_p^{-1}$, where τ_p is the momentum scattering lifetime for a spin-conserving process. The T^2-dependence originates from the fact that at higher temperature, thermally excited carriers are further away from band minima (K or K′) and will therefore scatter more efficiently. However, the predicted T^2 dependence does not describe the strong observed variation with temperature, which presumably arises from the temperature dependence of τ_p^{-1}. Indeed, a thermally activated temperature dependence is expected for phonon-assisted intervalley scattering at low temperatures, and the experimental activation energy of about 20 meV agrees with WSe_2 phonon energy (at the K point) required for intervalley scattering[96]. Phonon-assisted intervalley scattering, accompanied by spin flip through the Elliott–Yafet mechanism, can thus account for the observed spin–valley depolarization of holes.

The important role of K-point phonons in intervalley scattering is also supported by a recent resonant Raman study[96], which reveals second-order Raman signals (peaks p1 to p4 in Fig. 5c) assigned to K-point phonons through a doubly resonant Raman scattering process. This observation suggests a strong interaction between charge carriers and K-point phonons, which greatly enhances their second-order Raman signals through the doubly resonant Raman process illustrated in Fig. 5d.

Spin–valley transport

The efficient generation of pure spin–valley imbalance in hole-doped WSe_2/WS_2 heterostructures provides a convenient way to create pure spin–valley current (Fig. 6a), which lies in the heart of spin–valleytronic devices. Jin et al. performed space-and-time-resolved pump–probe spectroscopy to track the evolution of the spin–valley imbalance and to image the flow of pure spin–valley diffusion currents (Fig. 6b)[95]. Figure 6c shows experimental results for a hole-doped WS_2/WSe_2 heterostructure at an initial electrostatic hole doping of $p_0 = 1 \times 10^{12}$ cm^{-2}. At zero time delay, the spin–valley imbalance matches the spatial profile of the pump beam

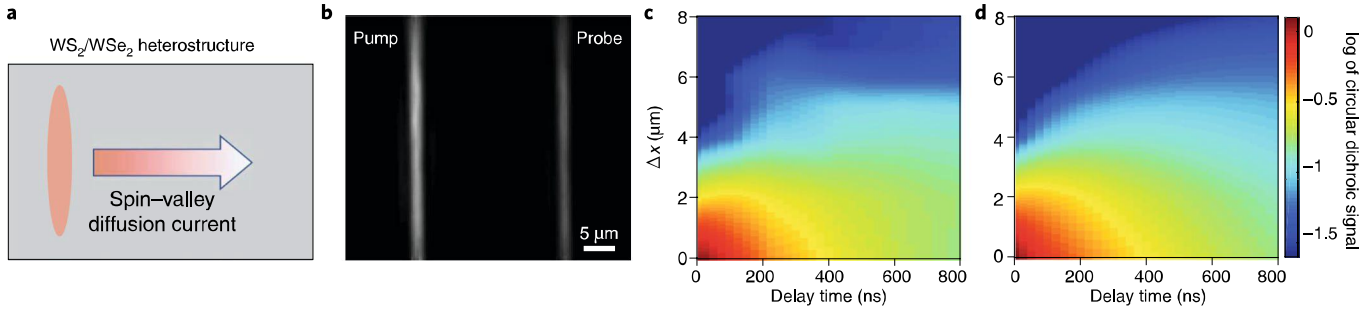

Fig. 6 | Spin–valley transport in a vdW heterostructure. a, Optical excitation of pure spin–valley imbalance at the left edge of a device will create a pure spin–valley diffusion current flowing to the right without any associated charge current. **b**, Experimental configuration for direct imaging of the spin–valley current flow with space-and-time resolved pump–probe spectroscopy, using pump and probe beams focused to lines on the sample at defined spatial separation. **c**,**d**, Experimentally measured spatio-temporal evolution of the pure valley imbalance in the heterostructure (**c**), and a simulation of the results using a diffusion–decay model (**d**) for an initial hole doping of 10^{12} cm^{-2}. Reproduced from ref. [95], AAAS.

(half-width of approximately 1.5 μm); the signal is negligible for pump–probe separations greater than 3 μm, as expected based on the convolution with the spatial profile of the probe. At finite delay time, the spin–valley imbalance diffuses out of the excitation region, generating a pure spin–valley current. This leads to a strong decrease and increase, respectively, of signal in regions near and away from the pump beam. The spin–valley current propagates to distances over 8 μm within 800 ns. Such direct imaging of the experimental spin–valley current flow (Fig. 6c) allows us to determine important physical parameters by comparison with a diffusion-decay model (Fig. 6d). We infer a diffusion constant of $D = 0.2$ cm^2 s^{-1} and a spin–valley lifetime of $\tau = 20$ μs, and deduce a spin–valley diffusion length of $l = \sqrt{D\tau} = 20$ μm.

The efficient generation of spin–valley current with remarkably large current densities reflects the nearly ideal conversion of photogenerated excitons into a spin–valley imbalance. Still higher spin–valley currents may be achievable in TMDC heterostructures by increasing the initial hole doping level to enable stronger optical pumping, as well as by improving the device quality to enhance the diffusivity. The long spin–valley lifetimes and diffusion lengths of valley-polarized holes in TDMC heterostructures hold promise for the generation, transport and detection of spin–valley information and open exciting opportunities for the realization of future spintronic and valleytronic devices.

Concluding remarks

Despite the rapid progress in the study of excited states in van der Waals heterostructures summarized above, many outstanding questions remain in understanding charge transfer processes and the spin and valley relaxation dynamics.

A complete picture of the underlying mechanism for the charge transfer process in TMDC heterostructures remains elusive. First, the mechanisms developed so far do not fully account for the Coulombic interactions between electrons and holes, despite the existence of strongly bound excitons both in the TMDC monolayers[8,97,98] and in the heterostructures[40]. Although one can argue that the excitonic states are superpositions of the quasiparticle band states and, hence, are affected similarly, a quantitative picture in which excitonic correlations are taken into account remains a theoretical challenge. In this context, it would also be interesting to learn whether the dielectric environment of the heterostructure, which affects the excitonic interactions, also significantly influences the rate and efficiency of charge transfer processes. In addition, the fact that changes in the dielectric screening of Coulombic interactions in TMDCs modify the quasiparticle band structure may provide a route to test the role of the Q and Γ valleys in charge transfer processes. Second, the time-domain probes of charge transfer have been limited in their temporal resolution by the instrumental response function and have not generally yielded precise charge transfer times. In addition, optical measurements, with their limited spatial resolution, average over moiré patterns formed between the two layers. This may lead to a washing out of predicted trends for charge transfer times. Overcoming these limitations by improved temporal resolution and/or spatial resolution (such as through near-field techniques) would provide important experimental information to inform and test theoretical models.

Similarly, many outstanding questions exist regarding spin and valley dynamics in TMDC heterostructures. Much more work is required to understand fully their intrinsic dynamics in TMDC heterostructures and the dependence of the dynamics on the constituent TMDC materials, their relative crystallographic alignment and their stacking order in multilayers. It remains, for example, unclear what factors define the ultimate limit for the spin–valley lifetime in TMDC heterostructures; also unknown are the roles played by defects, edges and grain boundaries, as well as possible effects from large-period moiré superlattices formed in TMDC heterostructures with small twist angles.

Online content

Any methods, additional references, Nature Research reporting summaries, source data, statements of data availability and associated accession codes are available at https://doi.org/10.1038/s41565-018-0298-5.

Received: 5 June 2018; Accepted: 5 October 2018;
Published online: 5 November 2018

References

1. Hunt, B. et al. Massive Dirac fermions and Hofstadter butterfly in a van der Waals heterostructure. *Science* **340**, 1427–1430 (2013).
2. Ponomarenko, L. A. et al. Cloning of Dirac fermions in graphene superlattices. *Nature* **497**, 594–597 (2013).
3. Dean, C. R. et al. Hofstadter's butterfly and the fractal quantum Hall effect in moiré superlattices. *Nature* **497**, 598–602 (2013).
4. Spanton, E. M. et al. Observation of fractional Chern insulators in a van der Waals heterostructure. *Science* **360**, 62–66 (2018).
5. Cao, Y. et al. Unconventional superconductivity in magic-angle graphene superlattices. *Nature* **556**, 43 (2018).
6. Cao, Y. et al. Correlated insulator behaviour at half-filling in magic-angle graphene superlattices. *Nature* **556**, 80–84 (2018).
7. Chen, G. et al. Gate-tunable Mott insulator in trilayer graphene–boron nitride moiré superlattice. Preprint at https://arxiv.org/abs/1803.01985 (2018).
8. Chernikov, A. et al. Exciton binding energy and nonhydrogenic Rydberg series in monolayer WS_2. *Phys. Rev. Lett.* **113**, 076802 (2014).
9. Ye, Z. L. et al. Probing excitonic dark states in single-layer tungsten disulphide. *Nature* **513**, 214–218 (2014).

10. Xiao, D., Liu, G. B., Feng, W. X., Xu, X. D. & Yao, W. Coupled spin and valley physics in monolayers of MoS_2 and other group-VI dichalcogenides. *Phys. Rev. Lett.* **108**, 196802 (2012).
11. Xu, X. D., Yao, W., Xiao, D. & Heinz, T. F. Spin and pseudospins in layered transition metal dichalcogenides. *Nat. Phys.* **10**, 343–350 (2014).
12. Komsa, H. P. & Krasheninnikov, A. V. Electronic structures and optical properties of realistic transition metal dichalcogenide heterostructures from first principles. *Phys. Rev. B* **88**, 085318 (2013).
13. Gong, C. et al. Band alignment of two-dimensional transition metal dichalcogenides: application in tunnel field effect transistors. *Appl. Phys. Lett.* **103**, 053513 (2013).
14. Terrones, H., Lopez-Urias, F. & Terrones, M. Novel hetero-layered materials with tunable direct band gaps by sandwiching different metal disulfides and diselenides. *Sci. Rep.* **3**, 1549 (2013).
15. Stormer, H. L., Dingle, R., Gossard, A. C., Wiegmann, W. & Sturge, M. D. 2-dimensional electron-gas at a semiconductor–semiconductor interface. *Solid State Commun.* **29**, 705–709 (1979).
16. Bellus, M. Z. et al. Type-I van der Waals heterostructure formed by MoS_2 and ReS_2 monolayers. *Nanoscale Horiz.* **2**, 31–36 (2017).
17. Chiu, M. H. et al. Determination of band alignment in the single-layer MoS_2/WSe_2 heterojunction. *Nat. Commun.* **6**, 7666 (2015).
18. Ozcelik, V. O., Azadani, J. G., Yang, C., Koester, S. J. & Low, T. Band alignment of two-dimensional semiconductors for designing heterostructures with momentum space matching. *Phys. Rev. B* **94**, 035125 (2016).
19. Hong, X. P. et al. Ultrafast charge transfer in atomically thin MoS_2/WS_2 heterostructures. *Nat. Nanotech.* **9**, 682–686 (2014).
20. Wang, K. et al. Interlayer coupling in twisted WSe_2/WS_2 bilayer heterostructures revealed by optical spectroscopy. *ACS Nano* **10**, 6612–6622 (2016).
21. Kozawa, D. et al. Evidence for fast interlayer energy transfer in $MoSe_2$/WS_2 heterostructures. *Nano Lett.* **16**, 4087–4093 (2016).
22. Zhang, C. X. et al. Systematic study of electronic structure and band alignment of monolayer transition metal dichalcogenides in Van der Waals heterostructures. *2D Mater.* **4**, 015026 (2017).
23. Debbichi, L., Eriksson, O. & Lebegue, S. Electronic structure of two-dimensional transition metal dichalcogenide bilayers from ab initio theory. *Phys. Rev. B* **89**, 205311 (2014).
24. Zhang, J. F., Xie, W. Y., Zhao, J. J. & Zhang, S. B. Band alignment of two-dimensional lateral heterostructures. *2D Mater.* **4**, 015038 (2017).
25. Qiu, D. Y., da Jornada, F. H. & Louie, S. G. Screening and many-body effects in two-dimensional crystals: monolayer MoS_2. *Phys. Rev. B* **93**, 235435 (2016).
26. Wilson, N. R. et al. Determination of band offsets, hybridization, and exciton binding in 2D semiconductor heterostructures. *Sci. Adv.* **3**, e1601832 (2017).
27. Hill, H. M., Rigosi, A. F., Rim, K. T., Flynn, G. W. & Heinz, T. F. Band alignment in MoS2/WS2 transition metal dichalcogenide heterostructures probed by scanning tunneling microscopy and spectroscopy. *Nano Lett.* **16**, 4831–4837 (2016).
28. Ceballos, F., Bellus, M. Z., Chiu, H. Y. & Zhao, H. Ultrafast charge separation and indirect exciton formation in a MoS_2–$MoSe_2$ van der Waals heterostructure. *ACS Nano* **8**, 12717–12724 (2014).
29. Heo, H. et al. Interlayer orientation-dependent light absorption and emission in monolayer semiconductor stacks. *Nat. Commun.* **6**, 7372 (2015).
30. Zhu, H. M. et al. Interfacial charge transfer circumventing momentum mismatch at two-dimensional van der Waals heterojunctions. *Nano Lett.* **17**, 3591–3598 (2017).
31. Ji, Z. H. et al. Robust stacking-independent ultrafast charge transfer in MoS_2/WS_2 bilayers. *ACS Nano* **11**, 12020–12026 (2017).
32. Chen, H. L. et al. Ultrafast formation of interlayer hot excitons in atomically thin MoS_2/WS_2 heterostructures. *Nat. Commun.* **7**, 12512 (2016).
33. Ceballos, F., Ju, M. G., Lane, S. D., Zeng, X. C. & Zhao, H. Highly efficient and anomalous charge transfer in van der Waals trilayer semiconductors. *Nano Lett.* **17**, 1623–1628 (2017).
34. Pan, S. D., Ceballos, F., Bellus, M. Z., Zereshki, P. & Zhao, H. Ultrafast charge transfer between $MoTe_2$ and MoS_2 monolayers. *2D Mater.* **4**, 015033 (2017).
35. Xu, W. G. et al. Correlated fluorescence blinking in two-dimensional semiconductor heterostructures. *Nature* **541**, 62–67 (2017).
36. Ceballos, F., Bellus, M. Z., Chiu, H. Y. & Zhao, H. Probing charge transfer excitons in a $MoSe_2$–WS_2 van der Waals heterostructure. *Nanoscale* **7**, 17523–17528 (2015).
37. Li, Y. Y. et al. Ultrafast interlayer electron transfer in incommensurate transition metal dichalcogenide homobilayers. *Nano Lett.* **17**, 6661–6666 (2017).
38. Rivera, P. et al. Observation of long-lived interlayer excitons in monolayer $MoSe_2$–WSe_2 heterostructures. *Nat. Commun.* **6**, 6242 (2015).
39. Rigosi, A. F., Hill, H. M., Li, Y. L., Chernikov, A. & Heinz, T. F. Probing interlayer interactions in transition metal dichalcogenide heterostructures by optical spectroscopy: MoS_2/WS_2 and $MoSe_2$/WSe_2. *Nano Lett.* **15**, 5033–5038 (2015).
40. Lee, C.-H. et al. Atomically thin p–n junctions with van der Waals heterointerfaces. *Nat. Nanotech.* **9**, 676–681 (2014).
41. Robert, C. et al. Exciton radiative lifetime in transition metal dichalcogenide monolayers. *Phys. Rev. B* **93**, 205423 (2016).
42. Xu, W. S. et al. Determining the optimized interlayer separation distance in vertical stacked 2D WS_2:hBN:MoS_2 heterostructures for exciton energy transfer. *Small* **14**, 1703727 (2018).
43. Mak, K. F., Lee, C., Hone, J., Shan, J. & Heinz, T. F. Atomically thin MoS_2: a new direct-gap semiconductor. *Phys. Rev. Lett.* **105**, 136805 (2010).
44. Splendiani, A. et al. Emerging photoluminescence in monolayer MoS_2. *Nano Lett.* **10**, 1271–1275 (2010).
45. Zhu, X. Y. et al. Charge transfer excitons at van der Waals interfaces. *J. Am. Chem. Soc.* **137**, 8313–8320 (2015).
46. Wang, H. et al. The role of collective motion in the ultrafast charge transfer in van der Waals heterostructures. *Nat. Commun.* **7**, 11504 (2016).
47. Zhang, J. et al. Interlayer-state-coupling dependent ultrafast charge transfer in MoS_2/WS_2 bilayers. *Adv. Sci.* **4**, 1700086 (2017).
48. Long, R. & Prezhdo, O. V. Quantum coherence facilitates efficient charge separation at a MoS_2/$MoSe_2$ van der Waals junction. *Nano Lett.* **16**, 1996–2003 (2016).
49. Li, L. Q., Long, R. & Prezhdo, O. V. Charge separation and recombination in two-dimensional MoS_2/WS_2: time-domain ab initio modeling. *Chem. Mater.* **29**, 2466–2473 (2017).
50. Kang, J., Li, J. B., Li, S. S., Xia, J. B. & Wang, L. W. Electronic structural moiré pattern effects on MoS_2/$MoSe_2$ 2D heterostructures. *Nano Lett.* **13**, 5485–5490 (2013).
51. Tong, Q. J. et al. Topological mosaics in moiré superlattices of van der Waals heterobilayers. *Nat. Phys.* **13**, 356–362 (2017).
52. Wang, Y., Wang, Z., Yao, W., Liu, G. B. & Yu, H. Y. Interlayer coupling in commensurate and incommensurate bilayer structures of transition-metal dichalcogenides. *Phys. Rev. B* **95**, 115429 (2017).
53. Zheng, Q. J. et al. Phonon-assisted ultrafast charge transfer at van der Waals heterostructure interface. *Nano Lett.* **17**, 6435–6442 (2017).
54. Jin, C. H. et al. On optical dipole moment and radiative recombination lifetime of excitons in WSe_2. *Adv. Funct. Mater.* **27**, 1601741 (2017).
55. Zhang, X. X., You, Y. M., Zhao, S. Y. F. & Heinz, T. F. Experimental evidence for dark excitons in monolayer WSe_2. *Phys. Rev. Lett.* **115**, 257403 (2015).
56. Korn, T., Heydrich, S., Hirmer, M., Schmutzler, J. & Schuller, C. Low-temperature photocarrier dynamics in monolayer MoS_2. *Appl. Phys. Lett.* **99**, 102109 (2011).
57. Amani, M. et al. Near-unity photoluminescence quantum yield in MoS_2. *Science* **350**, 1065–1068 (2015).
58. Moody, G. et al. Intrinsic homogeneous linewidth and broadening mechanisms of excitons in monolayer transition metal dichalcogenides. *Nat. Commun.* **6**, 8315 (2015).
59. Lagarde, D. et al. Carrier and polarization dynamics in monolayer MoS_2. *Phys. Rev. Lett.* **112**, 047401 (2014).
60. Wang, Q. S. et al. Valley carrier dynamics in mono layer molybdenum disulfide from helicity-resolved ultrafast pump–probe spectroscopy. *ACS Nano* **7**, 11087–11093 (2013).
61. Hao, K. et al. Direct measurement of exciton valley coherence in monolayer WSe_2. *Nat. Phys.* **12**, 677–682 (2016).
62. Mai, C. et al. Many-body effects in valleytronics: direct measurement of valley lifetimes in single-layer MoS_2. *Nano Lett.* **14**, 202–206 (2014).
63. Zhu, C. R. et al. Exciton valley dynamics probed by Kerr rotation in WSe_2 monolayers. *Phys. Rev. B* **90**, 161302(R) (2014).
64. Mak, K. F., He, K. L., Shan, J. & Heinz, T. F. Control of valley polarization in monolayer MoS_2 by optical helicity. *Nat. Nanotech.* **7**, 494–498 (2012).
65. Zeng, H. L., Dai, J. F., Yao, W., Xiao, D. & Cui, X. D. Valley polarization in MoS_2 monolayers by optical pumping. *Nat. Nanotech.* **7**, 490–493 (2012).
66. Cao, T. et al. Valley-selective circular dichroism of monolayer molybdenum disulphide. *Nat. Commun.* **3**, 887 (2012).
67. Glazov, M. M. et al. Exciton fine structure and spin decoherence in monolayers of transition metal dichalcogenides. *Phys. Rev. B* **89**, 201302(R) (2014).
68. Yu, T. & Wu, M. W. Valley depolarization due to intervalley and intravalley electron–hole exchange interactions in monolayer MoS_2. *Phys. Rev. B* **89**, 205303 (2014).
69. Yu, H. Y., Liu, G. B., Gong, P., Xu, X. D. & Yao, W. Dirac cones and Dirac saddle points of bright excitons in monolayer transition metal dichalcogenides. *Nat. Commun.* **5**, 3876 (2014).
70. Maialle, M. Z., Silva, E. A. D. E. & Sham, L. J. Exciton spin dynamics in quantum-wells. *Phys. Rev. B* **47**, 15776–15788 (1993).
71. Hao, K. et al. Trion valley coherence in monolayer semiconductors. *2D Mater.* **4**, 025105 (2017).
72. Volmer, F. et al. Intervalley dark trion states with spin lifetimes of 150 ns in WSe_2. *Phys. Rev. B* **95**, 235408 (2017).
73. Plechinger, G. et al. Trion fine structure and coupled spin–valley dynamics in monolayer tungsten disulfide. *Nat. Commun.* **7**, 12715 (2016).

74. Zhang, X. X. et al. Magnetic brightening and control of dark excitons in monolayer WSe_2. *Nat. Nanotech.* **12**, 883–888 (2017).
75. Jiang, C. Y. et al. Microsecond dark-exciton valley polarization memory in two-dimensional heterostructures. *Nat. Commun.* **9**, 753 (2018).
76. You, Y. M. et al. Observation of biexcitons in monolayer WSe_2. *Nat. Phys.* **11**, 477–481 (2015).
77. Chen, S., Goldstein, T., Taniguchi, T., Watanabe, K. & Yan, J. Coulomb-bound four- and five-particle valleytronic states in an atomically-thin semiconductor. *Nat. Commun.* **9**, 3717 (2018).
78. Dey, P. et al. Gate-controlled spin–valley locking of resident carriers in WSe_2 monolayers. *Phys. Rev. Lett.* **119**, 137401 (2017).
79. Song, X. L., Xie, S. E., Kang, K., Park, J. & Sih, V. Long-lived hole spin/valley polarization probed by Kerr rotation in monolayer WSe_2. *Nano Lett.* **16**, 5010–5014 (2016).
80. Hsu, W. T. et al. Optically initialized robust valley-polarized holes in monolayer WSe_2. *Nat. Commun.* **6**, 8963 (2015).
81. Yang, L. Y. et al. Long-lived nanosecond spin relaxation and spin coherence of electrons in monolayer MoS_2 and WS_2. *Nat. Phys.* **11**, 830–834 (2015).
82. Fang, H. et al. Strong interlayer coupling in van der Waals heterostructures built from single-layer chalcogenides. *Proc Natl Acad. Sci. USA* **111**, 6198–6202 (2014).
83. Nagler, P. et al. Interlayer exciton dynamics in a dichalcogenide monolayer heterostructure. *2D Mater.* **4**, 025112 (2017).
84. Rivera, P. et al. Valley-polarized exciton dynamics in a 2D semiconductor heterostructure. *Science* **351**, 688–691 (2016).
85. Hsu, W. T. et al. Negative circular polarization emissions from $WSe_2/MoSe_2$ commensurate heterobilayers. *Nat. Commun.* **9**, 1356 (2018).
86. Hanbicki, A. T. et al. Double indirect interlayer exciton in a $MoSe_2/WSe_2$ van der Waals heterostructure. *ACS Nano* **12**, 4719 (2018).
87. Ciarrocchi, A. et al. Control of interlayer excitons in two-dimensional van der Waals heterostructures. Preprint at https://arxiv.org/abs/1803.06405 (2018).
88. Yu, H. Y., Wang, Y., Tong, Q. J., Xu, X. D. & Yao, W. Anomalous light cones and valley optical selection rules of interlayer excitons in twisted heterobilayers. *Phys. Rev. Lett.* **115**, 187002 (2015).
89. Yu, H. Y., Liu, B. L. & Yao, W. Brightened spin-triplet interlayer excitons and optical selection rules in van der Waals heterobilayers. *2D Mater.* **5**, 035021 (2018).
90. Miller, B. et al. Long-lived direct and indirect interlayer excitons in van der Waals heterostructures. *Nano Lett.* **17**, 5229–5237 (2017).
91. Kunstmann, J. et al. Momentum-space indirect interlayer excitons in transition-metal dichalcogenide van der Waals heterostructures. *Nat. Phys.* **14**, 801–805 (2018).
92. Wu, F. C., Lovorn, T. & MacDonald, A. H. Theory of optical absorption by interlayer excitons in transition metal dichalcogenide heterobilayers. *Phys. Rev. B* **97**, 035306 (2018).
93. Yu, H. Y., Liu, G. B., Tang, J. J., Xu, X. D. & Yao, W. Moiré excitons: from programmable quantum emitter arrays to spin–orbit-coupled artificial lattices. *Sci. Adv.* **3**, e1701696 (2017).
94. Kim, J. et al. Observation of ultralong valley lifetime in WSe_2/MoS_2 heterostructures. *Sci. Adv.* **3**, e1700518 (2017).
95. Jin, C. H. et al. Imaging of pure spin–valley diffusion current in WS_2/WSe_2 heterostructures. *Science* **360**, 893–896 (2018).
96. Carvalho, B. R. et al. Intervalley scattering by acoustic phonons in two-dimensional MoS_2 revealed by double-resonance Raman spectroscopy. *Nat. Commun.* **8**, 14670 (2017).
97. Hill, H. M. et al. Observation of excitonic Rydberg states in monolayer MoS_2 and WS_2 by photoluminescence excitation spectroscopy. *Nano Lett.* **15**, 2992–2997 (2015).
98. He, K. L. et al. Tightly bound excitons in monolayer WSe_2. *Phys. Rev. Lett.* **113**, 026803 (2014).

Acknowledgements

E.Y.M. acknowledges support from the US Department of Energy, Office of Science, Basic Energy Sciences, Materials Sciences and Engineering Division, under contract DE-AC02-76SF00515. T.F.H. acknowledges support from the AMOS programme, Chemical Sciences, Geosciences, and Biosciences Division, Basic Energy Sciences, US Department of Energy under contract DE-AC02-76-SF00515 and from the Betty and Gordon Moore Foundation's EPiQS Initiative through grant no. GBMF4545. O.K. acknowledges the support of the Rothschild Fellowship of Yad Hanadiv Fund, Israel, the Viterbi Fellowship of the Andrew and Erna Viterbi Department of Electrical Engineering, Technion, Israel, and the Betty and Gordon Moore Foundation's EPiQS Initiative through grant no. GBMF4545. F.W. and E.C.R. acknowledge support from the Director, Office of Science, Office of Basic Energy Sciences, Materials Sciences and Engineering Division of the US Department of Energy under contract no. DE-AC02-05-CH11231 (van der Waals heterostructures programme, KCWF16). C.J. acknowledges support from the National Science Foundation EFRI programme (EFMA-1542741). E.C.R acknowledges support from the Department of Defense through the National Defense Science & Engineering Graduate (NDSEG) Fellowship programme.

Additional information

Correspondence should be addressed to F.W. or T.F.H.